

Compressive strength of pile foundation concrete in permafrost environment in China

Xiaoxiao Wang^{a,b}, Chang Liu^b, Shuguang Liu^{a,c,*}, Changwang Yan^{c,*}, Ju Zhang^c, Heng Li^b

^a School of Materials Science and Engineering, Inner Mongolia University of Technology, Hohhot 010051, China

^b School of Civil Engineering, Inner Mongolia University of Technology, Hohhot 010051, China

^c School of Mining and Technology, Inner Mongolia University of Technology, Hohhot 010051, China

HIGHLIGHTS

- Effect of icing content on compressive strength was studied.
- The law of pore icing was analyzed.
- The variation law of pore structure was investigated.
- A prediction model of compressive strength in Permafrost environment was established.

ARTICLE INFO

Article history:

Received 10 September 2019

Received in revised form 14 January 2020

Accepted 12 February 2020

Keywords:

Permafrost region

Pore icing

Pile foundation concrete

Compressive strength

ABSTRACT

This study aimed to investigate the influence of low temperature ranging from $-20\text{ }^{\circ}\text{C}$ to $0\text{ }^{\circ}\text{C}$ on the compressive strength and pore structure of a certain pile foundation concrete in the permafrost regions in China. This study analyzed concrete microstructure by low-temperature SEM. To quantify the influence of freezing amount, the relationship model of the compressive strength of concrete in a low-temperature environment was established based on the theory of accumulative curve of liquid saturation. Compressive strength increased with decreasing temperature. This finding was due to the gradual decrease in the pore radius of the water-ice phase transformation of concrete, and the amount of ice increased. This condition forms a complete and compact ice body and concrete bond, which gradually reduces concrete porosity. The calculated value of concrete compressive strength model established under pore icing is consistent with the experimental value.

© 2020 Elsevier Ltd. All rights reserved.

1. Introduction

The Qinghai-Tibet Railway, also known as the “Road to the Sky,” crosses the world’s largest distance of permafrost area at 550 km [1]. The average and minimum temperatures in the permafrost area are below $0\text{ }^{\circ}\text{C}$ and ranging from $-16\text{ }^{\circ}\text{C}$ to $-20\text{ }^{\circ}\text{C}$ [2,3]. The total length of the bridge and tunnel is approximately 8% of the total length of the railway. The pile foundation of bridge engineering has been in the permafrost area for a long time. Thus, concrete is required to reach the design strength under low temperature conditions and permafrost regions. The strength of the pile foundation in the permafrost area is greatly significant to the safe use of the Qinghai-Tibet Railway. Therefore, the strength of the bridge

pile foundation structure in the permafrost region in China is studied in this paper. Compressive strength is an important basis for evaluating concrete strength. The strength of concrete exposed to different temperatures from $0\text{ }^{\circ}\text{C}$ to $-20\text{ }^{\circ}\text{C}$ needs to be studied, and the results provide a reliable basis for evaluating the performance of low temperature concrete structure of the pile foundation of the Qinghai-Tibet Railway Bridge Project.

At present, concrete is an excellent low-temperature building material [4,5] that has good mechanical properties [6]. For example, Lee GC [7], Hideo Kasami [8], and Chuanxing Wang [9] considered that the compressive strength and elasticity modulus of concrete with different strengths have been improved to some extent at low temperatures (in the range $-100\text{ }^{\circ}\text{C}$ to $0\text{ }^{\circ}\text{C}$). Takashi Miur [10], Luis A Montejo [11], and Xudong Shi [12] determined from tests and analysis that the change of the mechanical properties of low-temperature concrete (from $-196\text{ }^{\circ}\text{C}$ to $20\text{ }^{\circ}\text{C}$) is closely related to concrete strength grade, water content, and temperature

* Corresponding authors at: Inner Mongolia University of Technology, Hohhot, China.

E-mail addresses: liusg6011@126.com (S. Liu), ycw20031013@126.com (C. Yan).

interval. Chao Liu [13] established a mathematical model of the mechanical properties, water cement ratio, and pore saturation of low temperature concrete based on the Wiedemann pore Model [14]. The same team also conducted the quantitative analysis and model establishment from the aspects of concrete strength, water content, and low temperature, while studying mechanical properties of low-temperature concrete [6–12]. However, the models proposed by the researchers differ. Thus, further investigation of the strength model of low-temperature concrete is necessary.

When the temperature of concrete falls below 0 °C, concrete performance is improved by water freezing reinforcement [15]. Xiao Pingcai [16] showed that the ice in the pore of concrete improves the mechanical properties of concrete. Susanta Chatterji [17] concluded that the formation of acicular fiber ice crystals or short and solid ice crystals improves the mechanical properties by ice freezing. Therefore, the icing of concrete pore structure directly affects its mechanical properties. Given that cement-based materials are structures with complex pore [4,5,18], the formation of pore ice has been extensively studied. Marshall [4] summarized the law of pore ice formation from –20 °C to –160 °C based on the coefficient of thermal expansion and the experiment data of Helmuth [19]. Jiang Zhengwu [5,20] used differential scanning calorimeter and thermometry to characterize the icing process of pore water in cryogenic temperatures (–110 °C and –170 °C). The influence of sample saturation on pore volume and pore size distribution were studied from 0 °C to –50 °C [21]. The relationship between pore ice formation and the increase of low temperature strength must be further explored. In addition, two representative hypotheses have been proposed for the ice formation mechanism of pore ice, that is, homogenous nucleation and progressive penetration follow heterogeneous nucleation [22]. These hypotheses do not form a unified theory. Therefore, the relationship among the formation of pore ice, compressive strength, and ice formation mechanism of concrete pore structure at low temperature must be further evaluated.

Based on the research background of the permafrost regions of Qinghai-Tibet Railway in China, the effect of concrete pore icing on pore structure and compressive strength under low temperatures (from 0 °C to –20 °C) was studied. The mechanism of the change of compressive strength was then analyzed by using scanning electron microscopy (SEM) under low temperature environment. Finally, considering the influence of icing amount on concrete strength, a prediction model of concrete compressive strength at low temperature was established. This model provides a theoretical basis for predicting the service performance of pile foundation concrete materials in the permafrost regions in China.

2. Test overview

2.1. Materials

The cement used was Jidong P.O42.5 Portland cement; Fly ash was Class I fly ash [20]. The performance indexes of cement and chemical composition of fly ash could be found in the published literature [23]. The particle size distribution of cement and fly ash are presented in Fig. 1. The coarse aggregate was composed of 5–20 mm gravel with continuous gradation. The fine aggregate was natural river sand with 2.55 fine modulus, 2.17% mud content, 1590 kg/m³ bulk density, 2550 kg/m³ apparent density, and 2.31% moisture content. This aggregate has good particle gradation. The water reducer was naphthalene water reducer with 18% water reducing rate. The water was ordinary tap water. The mixture ratio and performance for concrete are shown in Table 1.

2.2. Test design and test method

The specimens were made in accordance with the requirement of Chinese Standard GB/T50081–200 [24]. The form removal of the specimens was used after pouring and molding and maintained in a stationary state for 24 h. The concrete was then placed in the standard curing room at 20 °C ± 2 °C and 95% ± 5% relative humidity for curing. After 28 days, six concrete specimens were removed at different temperatures, three of which were tested for compressive strength at different low temperatures, whereas the other three were tested for nuclear magnetic resonance (NMR).

Low-temperature strength test: First, 100 mm × 100 mm × 100 mm concrete specimens cured for 28 days were saturated in a vacuum for 24 h by using a vacuum saturation device at 0.1 MPa vacuum pressure. The specimens were then placed into high-low temperature chamber for cooling. The temperature and humidity were adjusted to 0 °C and 95%, respectively, and the sample was collected after the center temperature of the specimen had been reduced to 0 °C. To ensure that the test environment temperature remained at 0 °C, the temperature in the autonomously produced low temperature pressure tester was lowered in advance [25]. Finally, the concrete specimens were placed into stainless steel molds to test the compressive strength at 0 °C, and the concrete was then tested at –5, –10, –15, and –20 °C.

Pore structure test: The concrete cured for 28 days was then cored, the specimen was a 50 mm (diameter) × 50 mm (height) cylinder. The cylinder specimens were saturated with water in a vacuum for 1 day. The specimens were then soaked in distilled water for 24 h to prevent the influence of other mineral ions on the NMR instrument. To prevent the loss of moisture in the specimen during the measurement process, the specimen was wrapped underwater by using waterproof material before testing. Teflon tape was used in this test. The specimen was cooled in the high-low temperature chamber (the same as in step 1). Finally, the specimen was placed into the nuclear magnetic instrument at 11.0528 MHz resonance frequency and 32 °C ± 0.01 °C magnet temperature. The temperature control system was adjusted to 0, –5, –10, –15, and –20 °C, and the specimen was tested after 20 min of temperature balancing to observed the porosity and T_2 spectrum distribution at different temperatures. The pore diameter distribution was calculated in combination with the mercury intrusion method.

Microstructure test: The ≤10 mm wide and 3–5 mm thick specimens were removed from the interior of the concrete and scanned using an EVO MA 15/LS 15 Zeiss electron microscope at low temperature.

2.3. Principle of pore structure testing by NMR

NMR technology reflects the signal intensity [26,27] by receiving hydrogen proton signals from liquid water. The volume of the pores in porous media can be obtained by the signal calibration method, thus allowing the porosity of the porous media to be obtained. The ice relaxation time is relatively short. Thus, the ice signal levels cannot be measured by an NMR instrument, after which the signal level decreases when the specimen is under low-temperature. The change in NMR signal level can reflect the change of porosity and pore diameter distribution [28].

The relationship between relaxation time of fluids in pore and pore diameter can be showed as follows [29]:

$$\frac{1}{T_2} = \rho_2 \left(\frac{S}{V} \right) = \rho_2 \left(\frac{F_s}{r} \right) \quad (1)$$

where T_2 is transverse relaxation time; ρ_2 is the surface relaxation rate, nm/ms; $S/V = F_s/r$ is the specific surface area of the pore; F_s is

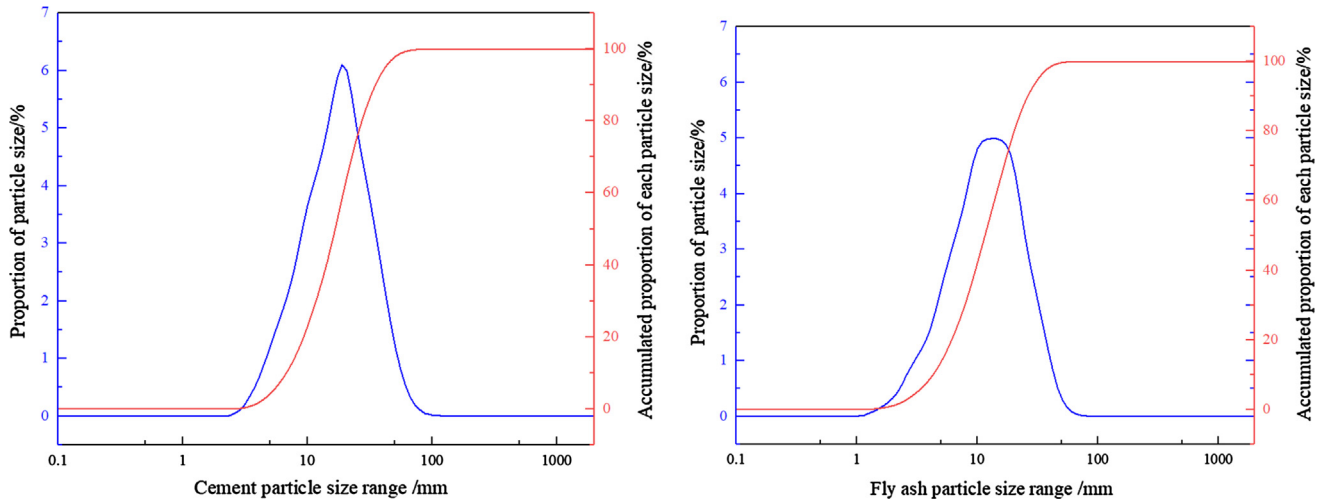


Fig. 1. Particle size distribution of cement and fly ash.

Table 1
Mixture ratio and performance for concrete.

The groups	Cement/Kg	Fly ash /Kg	Crushed stone /Kg	Sand/Kg	Water/Kg	Water-reducing agent /Kg	Air entraining agent/g	W/B	F_{28d} /MPa
C40	371	93	1204	567	160	9.0	46.4	0.34	40.9

the shape factor of the specimen pore that usually takes $F_s = 2$ for general cylindrical pores; $F_s = 3$ for spherical pores [30]; and r is the pore radius, nm .

The surface relaxation rate ρ_2 and shape factor F_s are constant for the same specimen; by setting $1/\rho_2 \cdot F_s = N$, the two sides of Formula (1) can be obtained using this logarithm:

$$LgT_2 - LgN = Lgr \quad (2)$$

By comparing the NMR T_2 distribution accumulation curve under different N values with the accumulative distribution curves of mercury injection pore size, the closest curve can calculate the N value [31]. Temperature slightly influences the parameters of the NMR of the specimen [32,33]. Thus, the N value is considered into the NMR T_2 spectrum of the specimen at different low temperatures to complete the conversion from the NMR T_2 spectrum to the pore size.

3. Test result and analysis

3.1. Development law of concrete compressive strength

When the pile foundation is buried in the permafrost environment for a long time, the temperature of concrete decreases to varying degrees. Fig. 2 shows that at $-20\text{ }^\circ\text{C} \leq T \leq 20\text{ }^\circ\text{C}$, the strength of pile foundation concrete increased with decreasing temperature. Three stages of development exists, as follows. The first stage is $0\text{ }^\circ\text{C} \leq T \leq 20\text{ }^\circ\text{C}$ (the slow growth stage of the strength of pile foundation concrete), in which the average compressive strength at 28 days is 40.9 MPa and then increased to 41.2 MPa when the temperature of pile foundation concrete is decreased to $0\text{ }^\circ\text{C}$. The second stage is $-15\text{ }^\circ\text{C} \leq T < 0\text{ }^\circ\text{C}$ (rapid growth stage of the strength of pile foundation concrete), in which the strength at $-5\text{ }^\circ\text{C}$, $-10\text{ }^\circ\text{C}$, and $-15\text{ }^\circ\text{C}$ is increased by 3.7%, 5.3%, and 12.0%, respectively, compared with the 28 day compressive strength. The third stage is $-20\text{ }^\circ\text{C} \leq T \leq -15\text{ }^\circ\text{C}$ (stabilization stage of the strength of pile foundation concrete), in which the strength of pile foundation at $-20\text{ }^\circ\text{C}$ is only increased by 2% compared with that at $-15\text{ }^\circ\text{C}$, and the strength of pile foundation concrete is stabilized.

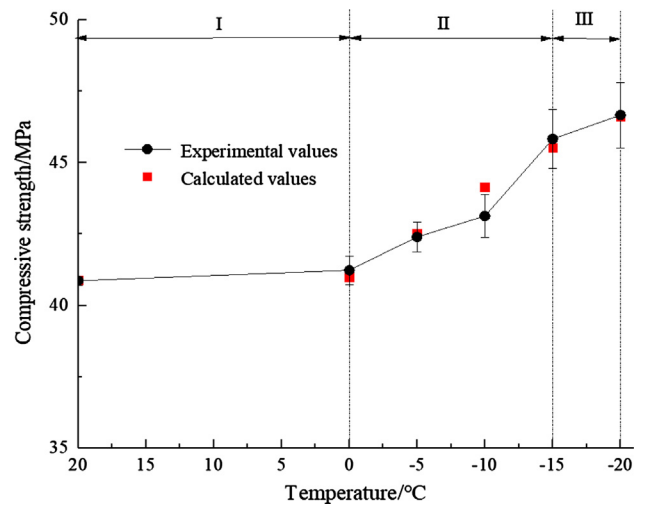


Fig. 2. Compressive strength of specimens under different temperatures.

Considering the above conditions, the icing amount and microstructure in the pores of pile foundation concrete changed under the permafrost environment, thereby resulting in the changes of the mechanical properties of materials.

3.2. Analysis of icing process in concrete pores

The temperature of pile foundation depends on permafrost in a permafrost area. Thus, the temperature and ice content of pile foundation concrete are the key to determine the strength of pile foundation concrete. The change of porosity can directly reflect the change of the ice content of pile foundation concrete pore solution. Fig. 3 shows the porosity of concrete at different temperatures. The porosity of pile foundation concrete decreased with reduced temperature, thereby indicating that the pore solution gradually iced. When the temperature of pile foundation concrete

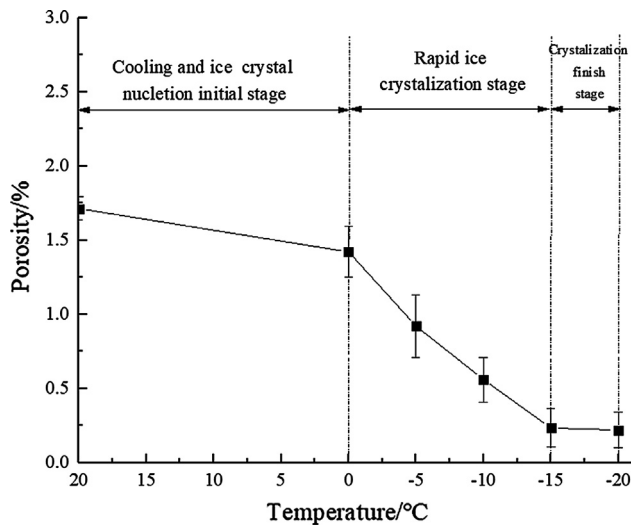


Fig. 3. Porosity of concrete at different temperatures.

dropped from 20 °C to 0 °C, the porosity of the specimens decreased by 17.0%. This finding showed that the water in the pores begins to freeze at $T = 0$ °C. However, most of the specimens are in a metastable state of uncrystallized nucleation [34], which is the initial stage of cooling and ice crystal nucleation. When the temperature of concrete is reduced from 0 °C to -15 °C, porosity decreases by 83.8%, and in this stage the content of pore water in the concrete rapidly decreases and freezes into ice, thereby denoting the rapid freezing stage. At continuous cooling down to -20 °C, the porosity of pile foundation concrete is stabilized, thereby indicating that the mass of icing of the pore water is stable at this stage, which is the completion stage of freezing.

3.3. Analysis of pore structure of concrete

The pore diameter distribution controls the strength, permeability, and durability of concrete [35]. Therefore, in this study, the pore size distribution was introduced to analyze the change law of the pore structure at low temperature. According to the definition of Rakesh Kumar pore structure [36], the pore diameter size is divided into the gel pores (<2 nm), gel interlayer pores (2 nm \ll R < 10 nm), fine capillary pores (10 nm < R < 50 nm), coarse capillary pores (50 nm < R < 500 nm), and non-capillary pores (R > 5000 nm).

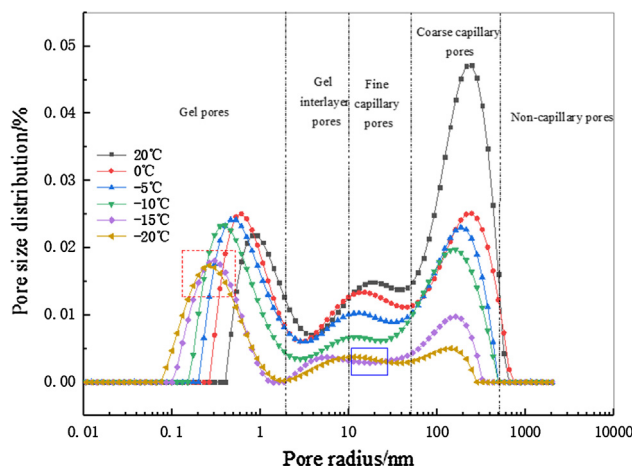


Fig. 4. Pore diameter distribution of specimens at different temperatures.

The pore size distribution of concrete at different temperatures is shown Fig. 4. When the temperature of concrete is decreased from 20 °C to 0 °C, the interval of capillary pores decreases, and the interval of gel pores slightly increases. Among these, 41.4% of coarse capillary pores and 20.1% of fine pores undergo a freezing phenomenon, whereas the 67.0% capillary pore solution remains in a liquid state. This condition indicates that the capillary pores first freeze, though not completely, when the pore structure is decreased to the freezing point. This is due to the fact that the water of capillary pores is physically bound by hydrated calcium silicate gels (C-S-H), which reduces the freezing point [37]. In addition, the capillary pores cannot freeze at the normal freezing point and are in the initial state of ice crystallization (ice-water mixture state), whereas the pore solution is ice-separated. This property results in the irregular decrease of the capillary pore radius and increases the “false appearance” of the gel pore solution. Three types of moisture are found in cement pastes that are restrained. The degree of firmness is in the following order: fine pore water < absorbed water of gel pores < interlayer water of C-S-H [38]. This finding is due to the fact that the coarse capillary pores are first frozen with a large amount of ice with the continuous decrease in temperature, and the phase change ice gradually transitions to fine pores (10 nm < R < 40 nm). When the temperature drops to -15 °C, the pore solution (10 nm < R < 500 nm) freezes rapidly, and 81.4% of the capillary pores are frozen. However, some of the capillary pores are not completely frozen due to the interfacial pre-thawing effect [39]. A layer of unfrozen water film of nano-scale forms, and this layer is between pore wall and ice body in frozen capillary pores [40]. When the temperature descend to -20 °C, only the 0.05 mm³ pore solution is frozen, and the freezing of the pore solution is stabilized.

From the change rule of the gel pores in Fig. 4 (marked with the red dotted line in the figure), when the concrete was below 0 °C, the pore size of the gel pores moved to the left with decreasing temperature. This finding indicated that the gel pores size decreases. Water in the gel pores didn't freeze at -78 °C and above [41]. When saturated concrete is reduced to -5, -10, -15 and -20 °C, the moisture of the gel pores existed in the form of super-cooled water and remained in a liquid state the entire time, whereas the water in the capillary pores froze. This phenomenon resulted in the thermodynamic non-equilibrium between the frozen water of capillary pores and super-cooled water of the gel pores [41,42]. The difference of the entropy between the ice body and super-cooled water promotes the migration of super-cooled water to a lower energy state, which then forms the ice in the capillary pore [43]. This phenomenon also increases the volume of capillary pores within the pore size range of 10–30 nm at -20 °C (shown in the blue box in the figure), and the capillary pores remain frozen at -15 °C and -20 °C.

3.4. Interaction relationship among the Icing, pore Structure, and compressive strength

The freezing phenomena of concrete at different temperatures were observed by SEM after processing the concrete specimen obtained 20 mm away from the specimen surface, as shown in Fig. 5. When the temperature drops to 4.1 °C, a small amount of ice crystals (marked by the red dotted lines) appear on the surface of the concrete, exhibiting needle-like or rod-like aggregation. The surface also shows irregular flocculent, needle-like, and sheet-like morphology (marked by the red solid lines in the figure), forming irregular layered space without evident sharp edges and angles. This finding can be determined from the morphology to be C-H-S polymer. In this temperature stage, many internal pores (marked with yellow lines in the figure) that are relatively loose are found.

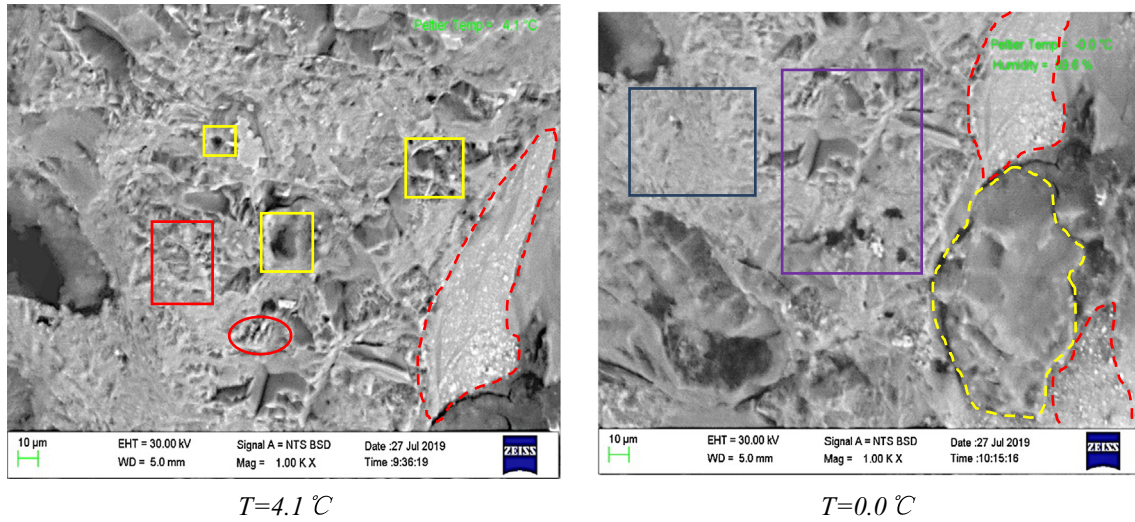


Fig. 5. Scanning electron microscope (SEM) photographs of concrete at different temperatures.

At $T = 0\text{ }^{\circ}\text{C}$, the capillary solution froze, as indicated by the yellow dotted lines in the figure. However, some unfrozen capillary pores remained, which is consistent with Litvan's development theory [37]. The water fixed by C-S-H in the capillary solution cannot freeze at the normal freezing point. The surface ice crystals continue to become larger. The acicular and flocculent morphology decreases, whereas the porosity decreases (marked by the purple solid lines in the figure), the integral ice surface appears (marked by blue line in the figure), and the concrete becomes denser overall, which improves the compressive strength.

Pile foundation concrete is in a permafrost environment (as shown in Fig. 6). By using a combination of SEM photographs (Fig. 5), pore structure (Section 3.3), icing (Section 3.2), and compressive strength (Section 3.1) of pile foundation concrete, the mechanism of mechanical strengthening of concrete was obtained. When the pile foundation concrete was attached to the permafrost environment, the solution of coarse capillary pores was partially frozen with decreasing temperature. As the temperature continued to decrease, the fine capillary pore solution icing and the super-cooled water in the gel pores are transferred to the capillary pores to increase the ice content. Ice is a high-strength material, and its bonding strength with concrete as a porous hydrophilic material is very high. Under the same conditions, the bonding strength of concrete and ice is much greater than the concrete, and the ice strengths [44]. Therefore, the strength of concrete is gradually improved by the self-strengthening of concrete strength and the cohesion of pore water freezing and concrete into a whole. In summary, the ice content of pile foundation concrete is the key to determine its compressive strength, and the amount of ice content depends on the variation of pore size distribution under different temperatures.

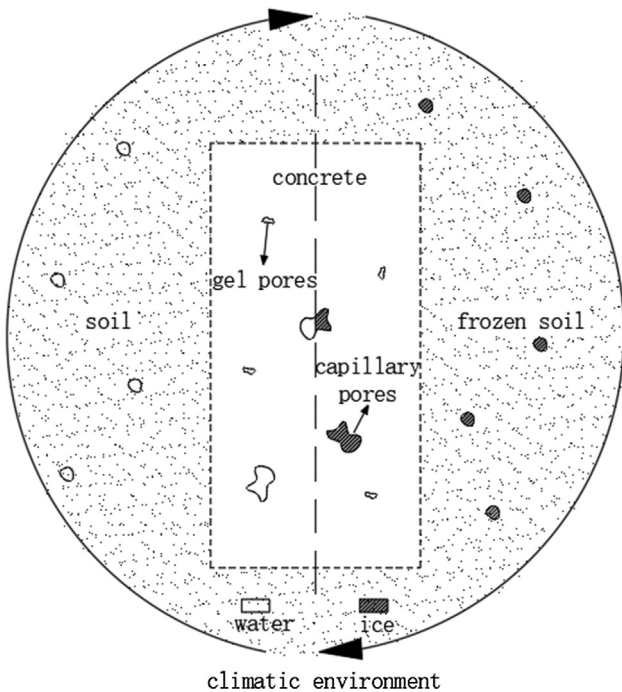


Fig. 6. Schematic of pile foundation concrete in permafrost environment. Pile foundation concrete is buried in a permafrost area, and the existence of permafrost is affected by the climate environment. When the climate temperature decreases, the frozen soil internally freezes. The temperature of the pile foundation concrete decreases with the temperature of the surrounding frozen soil, and the pore solution of the concrete freezes.

4. Prediction and analysis of concrete compressive strength in permafrost soil environment

4.1. Prediction model of concrete compressive strength considering the effect of pore icing

According to the variation law of compressive strength in a permafrost soil environment, the compressive strength can be divided into two parts under low temperature [13]. The formula for this is as follows:

$$f_c(T) = f_{c,28d} + \Delta f_c(T) \tag{3}$$

where $f_c(T)$ is the compressive strength of specimen at low temperature; $f_{c,28d}$ is the compressive strength at 28 days; and $\Delta f_c(T)$ is the increment of compressive strength under low temperature.

Fig. 7 shows concrete pore icing in a frozen soil environment. From a mesoscopic point of view, each phase composition of concrete can be divided into two parts before freezing: the solid (porosity is 0) and pore phases. After pore freezing, the pore phase can be composed of ice and free water (include non-free unfrozen water and free unfrozen water). The mechanical properties of solid

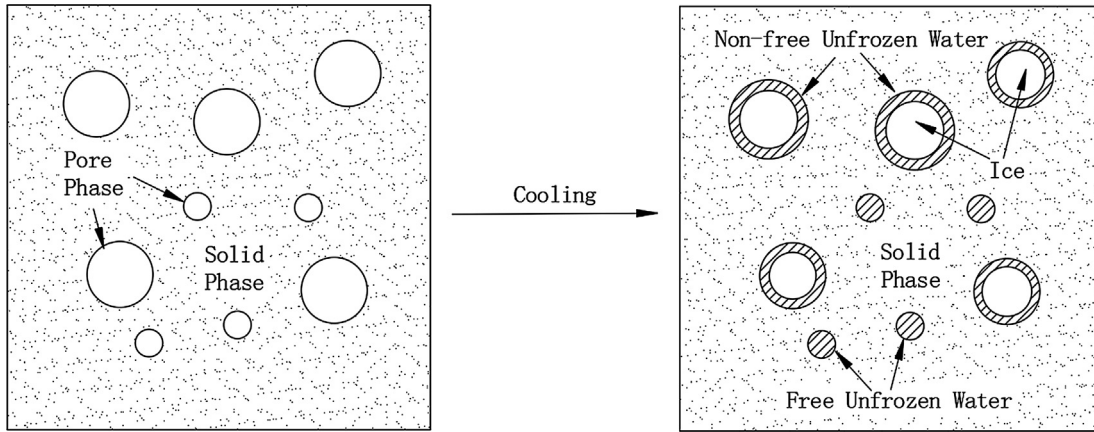


Fig. 7. Distribution of icing in the pores of concrete. Annotations: The freezing point of gel pore water is lower than that of free volume water, and the water in the pore remains liquid. This part of unfrozen pore water is called free unfrozen water. A layer of unfrozen water film of nano-scale forms between the pore wall and ice body in frozen capillary pores, which is called non-free unfrozen.

phase remain unchanged, and the strength of free water is neglected. Thus, the strength of ice directly affects the value of $\Delta f_c(T)$.

Assuming that the pore water saturation of concrete is the same and without considering the potential energy flow between the unfrozen pore water and the change of crystal morphology of the ice at different temperatures, the relationship between $\Delta f_c(T)$ and S_c is obtained as follows, in combination with the freezing characteristics of pore structure:

$$\Delta f_c(T) = \frac{f_{c,ice}(T) \times V_{ice}/H}{V_{concret}/H} = f_{c,ice}(T) \times S_c(T) \quad (4)$$

where $f_{c,ice}(T)$ is the ultimate compressive strength of ice under different temperatures; V_{ice} is the volume of ice; $V_{concret}$ is the volume of concrete; H is the height of the specimens; and $S_c(T)$ is the cumulative volume fraction of the ice.

4.2. Determination of model parameters

The relationship between ice compressive strength and temperature based on experimental data have been established [45,46]:

$$f_{c,ice}(T) = \begin{cases} 1.9684 \ln|T| + 0.3746, & 0^\circ \text{C} < T \leq -30^\circ \text{C} \\ 0.35, & T = 0^\circ \text{C} \end{cases} \quad (5)$$

For cement-based materials, pores that are larger than the critical pore size freeze at certain temperatures [47]. By ignoring the density difference between ice and water, Gibbs–Thomson equation can be obtained by the thermodynamic equilibrium between ice and liquid water, thereby requiring the chemical potential of the two phases to be equal [39]:

$$r = \frac{2\gamma_{cl}}{\sum_m(T_m - T)} \quad (6)$$

where γ_{cl} is the crystal-liquid interface energy; \sum_m is the melting entrop that is constant; $T_m = 0^\circ \text{C}$ is the freezing point of free volume water at atmospheric pressure; and T is the freezing temperature. Formula (6) indicates that r is the minimum pore radius for the occurrence of water–ice phase transformation at freezing temperature T .

The accumulative pore volume fraction $F(r)$ can be obtained by NMR and mercury injection tests, and the accumulative pore volume distribution function satisfies the following exponential function [48]:

$$F(r) = 1 - \exp(-m/r) \quad (7)$$

where m is the parameter related to pore distribution, nm.

By substituting Formula (6) into Formula (7), the cumulative volume fraction S_c of the ice at temperature $T < T_m$ is as follows:

$$S_c = F\left(r_f = \frac{2\gamma_{cl}}{\sum_m(T_m - T)}\right) = 1 - \exp\left(-\frac{m}{W}\Delta T\right) \quad (8)$$

where $W = \frac{2\gamma_{cl}}{\sum_m}$, and $\Delta T = T_m - T$, $\gamma_{cl} = 0.0409 \text{ J} \cdot \text{m}^{-2}$ and $\sum_m = 1.2 \text{ MPa} \cdot \text{K}^{-1}$ when $T = T_m = 237.15 \text{ K}$, then $W = 6.82 \times 10^{-8} \text{ m} \cdot ^\circ \text{C}$ [49,50].

At $T = 0^\circ \text{C}$, the concrete pore solution has frozen. By substituting the experimental data of Fig. 8 (Accumulated volume fraction of ice in pores) into Formula (8) and correcting the S_c , we can obtain the following:

$$S_c(T) = 1.170 - \exp\left[-\frac{m}{W}(T_m - T)\right] \quad (9)$$

where $S_c(T)$ is the cumulative volume fraction of ice and $m = 4.638$ is a parameter related to the pore distribution, nm.

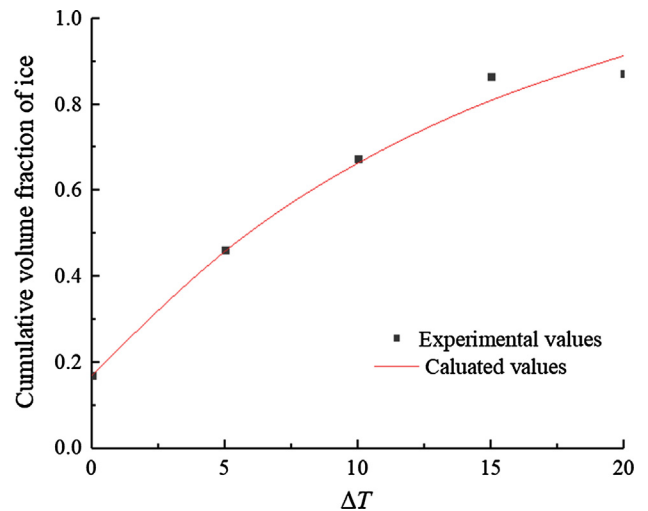


Fig. 8. Accumulated volume fraction of ice in pores.

Table 2
Comparison between the calculated compressive strength model and experimental in reference [5].

Source of date	Temperature /°C	Experimental data of compressive strength/MPa	Calculated data of compressive strength/MPa	Value errors
Jiang Zhengwu [5]	0	49.50	49.56	1.21%
	−5	51.38	50.63	1.45%
	−10	53.25	51.71	2.89%
	−15	55.13	52.64	4.51%
	−20	56.30	53.51	4.96%

4.3. Validation and analysis of model results

By substituting Formulas (5) and (9) into Formula (4) and combining these with Formula (3) to calculate the concrete compressive strength under low temperature, the calculated values and experimental values are shown in Fig. 2. The calculated value of strength at low temperature is consistent with the experimental value, and both show an increasing trend with decreasing temperature with a maximum error of only 2.4%.

The corresponding temperature in Table 2 is brought into the compressive strength model established in this paper. The calculated value of compressive strength in low temperature is very close to the measured value with a 1.21%–4.96% error range. This model shows that the strength of pile foundation concrete at low temperature can be determined by testing the amount of concrete icing that uses the compressive strength calculation model.

5. Conclusion

The work investigated the freezing law of concrete pore and the change law of compressive strength under the environment of permafrost regions in China (temperature range: from 0 °C to −20 °C), the conclusions were as follows:

- (1) The icing process in concrete pores can be divided into three following stages. First, the initial stage of cooling and ice crystal nucleation ($0\text{ °C} \leq T \leq 20\text{ °C}$) occur. This stage shows that the freezing of the capillary pores occurs first. Given the physical restraint of C-S-H, the freezing point of the capillary pores decreases, and the capillary pores do not freeze completely. Second, the rapid freezing stage ($-15\text{ °C} \leq T \leq 0\text{ °C}$) occurs. This stage shows that 81.4% of the capillary pores freeze, and the nano-scale unfrozen water film exists in the capillary pores due to the interface effect. Third, the completion stage of freezing ($-20\text{ °C} \leq T \leq -15\text{ °C}$) occurs. This stage shows that the supercooled water in the condensate pore migrates to the capillary pores due to the difference of entropy between the ice and supercooled water. This condition causes the minor freezing of the capillary pores at this stage.
- (2) The concrete compressive strength increases with the decrease of temperature. This phenomenon due to the increase of ice content in the pore structure, which alters the microstructure and improves the compactness and strength of the concrete.
- (3) The calculated value of the mechanical model established for the concrete compressive strength at low temperature is consistent with the experimental value.

CRedit authorship contribution statement

Xiaoxiao Wang: Investigation, Formal analysis, Writing - original draft. **Chang Liu:** Formal analysis, Validation. **Shuguang Liu:** Funding acquisition, Resources, Supervision, Writing - review & editing. **Changwang Yan:** Conceptualization, Supervision, Writing

- review & editing. **Ju Zhang:** Writing - review & editing. **Heng Li:** Writing - review & editing.

Declaration of Competing Interest

The authors declare that they have no known competing financial interests or personal relationships that could have appeared to influence the work reported in this paper.

Acknowledgements

This study was supported by the National Natural Science Foundation of China [grant No. 51609119, 51768041], and by program for Yong Talents of Science and Technology in Universities of Inner Mongolia Autonomous Region [grant No. NJYT-18-B24].

References

- [1] G.D. Cheng, Q.B. Wu, W. Ma, Innovative designs of permafrost roadbed for the Qinghai-Tibet Railway, *Sci. China Ser. E: Technol. Sci.* 52 (2009) 530–538.
- [2] Y. Ran, X. Li, G. Cheng, Distribution of permafrost in China: an overview of existing permafrost maps, *Permafrost Periglac. Process.* 23 (2012) 322–333.
- [3] Q.B. Wu, G.L. Jiang, P. Zhang, Assessing the permafrost temperature and thickness conditions favorable for the occurrence of gas hydrate in the Qinghai-Tibet Plateau, *Energy Convers. Manage.* 51 (2010) 783–787.
- [4] A.L. Marshall, Cryogenic concrete, *Cryogenics* 22 (1982) 555–565.
- [5] Z. Jiang, Z. Deng, X. Zhu, Increased strength and related mechanisms for mortars at cryogenic temperatures, *Cryogenics* 94 (2018) 5–13.
- [6] Z.W. Jiang, N. Zhang, X.Y. Li, State-of-art review on properties of concrete at cryogenic temperature overseas, *Mater. Rev.* 25 (2011) 1–4.
- [7] G.C. Lee, T.S. Shih, K.C. Chang, Mechanical properties of high-strength concrete at low temperature, *J. Cold Reg. Eng.* 2 (1988) 169–178.
- [8] H. Kasami, Y. Tanaka, Y. Kishima, Properties of concrete at very low temperatures, in: *Proc. 1st Int. Conf. on Cryogenic Concrete*, 1981, pp. 123–134.
- [9] C.X. Wang, J. Xie, H.J. Li, Experimental research on the properties of concrete under low-temperature, *Eng. Mech.* 28 (2011) 182–186.
- [10] T. Miura, The properties of concrete at very low temperatures, *Mater. Struct.* 22 (1989) 243–254.
- [11] L.A. Montejo, J.E. Sloan, M.J. Kowalsky, Cyclic response of reinforced concrete members at low temperatures, *J. Cold Reg. Eng.* 22 (2008) 79–102.
- [12] X.D. Shi, C. Ma, T.S. Zhang, Experimental study on compressive behavior of different strength grade concretes exposed to -190 °C, *Eng. Mech.* 34 (2017) 61–68.
- [13] C. Liu, Experimental Investigation on Mechanical Property of Concrete Exposed to Low Temperatures PhD Thesis, Tsinghua University, The China (2011).
- [14] G. Wiedemann, Zum Einfluss Tiefer Temperaturen auf Festigkeit und Verformung von Beton, PhD Thesis, Technical University of Braunschweig, the Germany; 1982.
- [15] X. Liu, M.H. Zhang, K.S. Chia, Mechanical properties of ultra-lightweight cement composite at low temperatures of 0 to −60 °C, *Cem. Concr. Compos.* 73 (2016) 289–298.
- [16] X.P. Cai, W.C. Yang, J. Yuan, Effect of low temperature on mechanical properties of concrete with different strength grade, *Key Eng. Mater.* 477 (2011) 308–312.
- [17] S. Chatterji, Aspects of the freezing process in a porous material–water system: part 1. Freezing and the properties of water and ice, *Cem. Concr. Res.* 29 (1999) 627–630.
- [18] M. Wu, B. Johannesson, Impact of sample saturation on the detected porosity of hardened concrete using low temperature calorimetry, *Thermochim Acta* 580 (2014) 66–78.
- [19] R.A. Helmuth, Capillary size restrictions on ice formation in hardened Portland cement pastes, in: *Paper VI-S2, Proc Fourth Int Symp on Chemistry of Cement*, Washington, 1960, pp. 855–869.
- [20] Z.W. Jiang, C. Zhang, Z.L. Deng, X.P. Zhu, W.T. Li, Thermal strain of cement-based materials under cryogenic temperatures and its freeze-thaw cycles using fibre Bragg grating sensor, *Cryogenics* 100 (2019) 1–10.
- [21] Z. Sun, G. Scherer, Pore size and shape in mortar by thermoporometry, *Cem. Concr. Res.* 40 (2010) 740–751.

- [22] X.X. Wang, Y. Wu, X.D. Shen, An experimental study of a freeze-thaw damage model of natural pumice concrete, *Powder Technol.* 339 (2018) 651–658, <https://doi.org/10.1016/j.powtec.2018.07.096>.
- [23] X.X. Wang, X.D. Shen, H.L. Wang, et al., Nuclear magnetic resonance analysis of freeze-thaw damage in natural pumice concrete, *Nuclear magnetic resonance analysis of freeze-thaw damage in natural pumice concrete*, *Mater. construcc.* 66 (322) (2016) e087, <https://doi.org/10.3989/mc.2016.v66.i32210.3989/mc.2016.09014>.
- [24] GB/T50081-2002, Standard for testing methods of mechanical properties of ordinary concrete, 2013.
- [25] X.X. Wang, S.G. Liu, C.W. Yan, H. Li, An experimental device and test method for controlling low temperature environment, the China, 201811628641.6, 2018.
- [26] K.R. Brownstein, C.E. Tarr, Spin-lattice relaxation in a system governed by diffusion, *J. Magn. Reson.* 26 (1977) 17–24.
- [27] B.D. Lowden, M.J. Porter, L.S. Powrie, T2 relaxation time versus mercury injection capillary pressure: Implications for NMR logging and reservoir characterisation, *European Petroleum Conference*, 20–22 October 1998.
- [28] X.X. Wang, X.D. Shen, H.L. Wang, Research on icing law of pore solution in natural pumice concrete, *Mater. Rep.* 31 (2017) 130–135.
- [29] C. Zhou, F. Ren, Q. Zeng, Pore-size resolved water vapor adsorption kinetics of white cement mortars as viewed from proton NMR relaxation, *Cem. Concr. Res.* 105 (2018) 31–43.
- [30] Y.D. Li, C. Yang, S. Feng, Method of studying pore diameter distribution of shale by nuclear magnetic resonance, *Geolog. Rev.* 63 (2017) 119–120.
- [31] H.B. Li, J.Y. Zhu, H.K. Guo, Methods of pore radius distribution by NMR T₂ spectrum conversion, *J. Spectroscopy* 25 (2008) 273–280.
- [32] I. Foley, S.A. Farooqui, R.L. Kleinberg, Effect of paramagnetic ions on NMR relaxation of fluids at solid surfaces, *J. Magn. Reson., Ser A* 123 (1996) 95–104.
- [33] L.L. Latour, R.L. Kleinberg, A. Sezginer, Nuclear magnetic resonance properties of rocks at elevated temperatures, *J. Colloid Interface Sci.* 150 (1992) 535–548.
- [34] R. Yang, E. Lemarchand, T. Fen-Chong, A micromechanics model for partial freezing in porous media, *Int. J. Solids Struct.* 75 (2015) 109–121.
- [35] C.Y. Zhang, Y. Cai, X.M. Kong, Influence of nano C-S-H on cement hydration, pore structure of hardened cement pastes and strength of concrete, *J. Chinese Ceramic Soc.* 47 (2019) 585–593.
- [36] R. Kumar, B.P. Bhattacharjee, Pore size distribution and in situ strength of concrete [J], *Cem. Concr. Res.* 33 (2003) 155–164.
- [37] G.G. Litvan, Phase transitions of adsorbates: IV, Mechanism of frost action in hardened cement paste, *J. Am. Ceram. Soc.* 55 (1972) 38–42.
- [38] P.K. Mehta, D. Paulo, J.M. Monteiro, *Concrete: Microstructure, Properties and Materials*, Fourth Edition., McGraw-Hill Education, 2014.
- [39] J.S. Wettlaufer, M.G. Worster, Premelting dynamics, *Annu. Rev. Fluid Mech.* 38 (2006) 427–452.
- [40] Q.S. Liu, S.B. Huang, Y.S. Kang, Study of unfrozen water content and frost heave model for saturated rock under low temperature, *Chinese J. Rock Mech. Eng.* 35 (2016) 2000–2012.
- [41] A.M. Neville, *Properties of Concrete*, Pitman Publishing, 1996, pp. 838–844.
- [42] T.C. Powers, Freezing effects in concrete, *Durability Concret.* 1 (1975) 332–338.
- [43] F. Gong, S. Jacobsen, Modeling of water transport in highly saturated concrete with wet surface during freeze/thaw, *Cem. Concr. Res.* 115 (2019) 294–307.
- [44] N. Neithalath, M.S. Sumanasooriya, O. Deo, Characterizing pore volume, sizes, and connectivity in pervious concretes for permeability prediction, *Mater. Charact.* 61 (2010) 802–813.
- [45] J. Wang, T. Yu, M. Huang, Experimental study on uniaxial unconfined compressive strength of river ice, *Low Temp. Build. Technol.* 1 (2007) 11–13.
- [46] F.D. Haynes, Temperature effect on the uniaxial strength of ice, *Int Port and Ocean Eng Upper Arctic Cond Conf*, 1980.
- [47] W.S. George, Crystallization in pores, *Cem. Concr. Res.* 29 (1999) 1347–1358.
- [48] O. Coussy, P.J.M. Monteiro, Poroelastic model for concrete exposed to freezing temperatures, *Cem. Concr. Res.* 38 (2008) 40–48.
- [49] M. Brun, A. Lallemand, J.F. Quinson, A new method for the simultaneous determination of the size and shape of pores: the thermoporometry, *Thermochim Acta* 21 (1977) 59–88.
- [50] V.F. Petrenko, R.W. Whitworth, *Physics of Ice*, 1st edition., Oxford UnivSersity Press, 1999.